CrossMark

RESEARCH PAPER

Electrokinetic motion of single nanoparticles in single PDMS nanochannels

Ran Peng[1] · Dongqing Li[1]

Abstract Electrokinetic motion of single nanoparticles in single nanochannels was studied systematically by image tracking method. A novel method to fabricate PDMS-glass micro/nanochannel chips with single nanochannels was presented. The effects of ionic concentration of the buffer solution, particle-to-channel size ratio and electric field on the electrokinetic velocity of fluorescent nanoparticles were studied. The experimental results show that the apparent velocity of nanoparticles in single nanochannels increases with the ionic concentration when the ionic concentration is low and decreases with the ionic concentration when the concentration is high. The apparent velocity decreases with the particle-to-channel size ratio (a/b). Under the condition of low electric fields, nanoparticles can hardly move in single nanochannels with a large particle-to-channel size ratio. Generally, the apparent velocity increases with the applied electric field linearly. The experimental study presented in this article is valuable for future research and applications of transport and manipulation of nanoparticles in nanofluidic devices, such as separation of charged nanoparticles and DNA molecules.

Keywords Electrokinetic motion · Nanoparticles · PDMS nanochannels · Particle-to-channel size ratio

✉ Dongqing Li
  dongqing@uwaterloo.ca

[1] Department of Mechanical and Mechatronics Engineering, University of Waterloo, Waterloo, ON N2L 3G1, Canada

1 Introduction

The phenomenon of electrophoresis describes the motion of charged colloidal particles suspended in electrolyte solutions in response to external applied electric fields (Li 2004; Masliyah and Bhattacharjee 2006) has long been applied to separate a mixture of charged particles or molecules practically by using porous media, such as gels (Unlu et al. 1997). The development of nanofabrication techniques today (Mijatovic et al. 2005; Xia et al. 2012; Duan et al. 2013) makes manipulation and transport of target molecules and particles in nanofluidic platforms possible. For example, stretching, separation and direct observation of DNAs (Napoli et al. 2010; Menard and Ramsey 2013; Yasui et al. 2013; Sackmann et al. 2014; Jeffet et al. 2016; Plesa et al. 2016) and proteins (Wang et al. 2005; Fu et al. 2007), sizing and detection of nanoparticles (Zhou et al. 2011; Davenport et al. 2012; Harms et al. 2015) by electrokinetically driven force in nanofluidics devices have been reported recently. However, to make full use of these techniques with high performance and efficiency, it is crucial to fully understand the mechanism of electrokinetic motion of nanoparticles or molecules in the nanoscale spaces, such as in straight nanochannels.

A large number of numerical and analytical models have been developed to study the electrophoresis behavior since the last century, and these models are based on different limiting assumptions and working conditions, such as domain boundary, particle shape and surface zeta potential, type of electrolyte solution and thickness of electric double layer (EDL). In the early years, Helmholtz–Smoluchowski and Debye–Huckel models for electrophoresis of particles in open boundaries assume particle motion in stationary liquids under the conditions of thin EDL ($ka \gg 1$) and thick EDL ($ka \ll 1$), respectively (Dukhin 1993; Delgado et al.

2007), where a is the radius of the particle, and k^{-1} is the Debye length. Two general formulas for the electrophoretic mobility of charged particles in concentrated electrolyte solutions and charged particles in extremely diluted electrolyte solutions were derived (Masliyah and Bhattacharjee 2006). These two formulas are bridged by Henry's function valid for arbitrary ka (Henry 1931) and further improved by Ohshima (1994, 1996) and Swan and Furst (2012). Modern theories focusing on the other working parameters and conditions have also been developed. These conditions can be divided into two branches, including the above-mentioned unbounded environment (Wiersema et al. 1966; Ohshima et al. 1983; Chen and Keh 1988) and the bonded domain which investigates the channel wall effects on the electrophoretic motion of particles. Particle motion near a flat plane (Keh and Anderson 1985; Keh and Chen 1988; Shugai and Carnie 1999), in rectangular channels (Movahed and Li 2012; Liu et al. 2016), cylindrical channels (Keh and Chiou 1996; Hsu and Chen 2007) with the conditions of thick EDL limit (Ennis and Anderson 1997; Hsu et al. 2004; Miloh and Boymelgreen 2014), thin EDL limit (O'Brien and Hunter 1981; Keh and Anderson 1985; Keh and Chen 1988; Hsu et al. 2012a) and arbitrary EDL thickness (Keh and Hsieh 2008; Chen and Keh 2013; Liu et al. 2014) has been studied. The thickness of EDL is dominated by the ionic concentration of the buffer solutions (Li 2004); however, pH values (Hsu et al. 2012b; Wang et al. 2013) and symmetry or asymmetry property of the ions (O'Brien and White 1978; Semenov et al. 2013; Nedelcu and Sommer 2014; Liu et al. 2016) also affect the electrophoretic behavior. For the cases of particle motion in cylindrical channels, generally, the particles move along the centerlines of the channels (Keh and Chiou 1996; Shugai and Carnie 1999; Tseng et al. 2013); however, the off-centerline effect has also been investigated (Zhang et al. 2009; Lee and Keh 2014; Liu et al. 2014). Zeta potential of the particle surfaces is another key parameter in the electrophoresis. Besides the general low zeta potential assumption (Ennis and Anderson 1997; Shugai and Carnie 1999; Hsu et al. 2004), particles with high zeta potential (Wiersema et al. 1966; O'Brien and White 1978; Liu et al. 2016), arbitrary zeta potential (Keh and Hsieh 2008) and particles with non-uniform zeta potential distribution (Qian et al. 2008; Wang and Keh 2009) have also been studied. In addition, electrophoresis models involving neutral particles and dielectric particles (Shugai and Carnie 1999; Miloh and Boymelgreen 2014) and particles made of soft materials (Ohshima 1995a, b; Hsu et al. 2012a; Chen and Keh 2013; Tseng et al. 2013), porous media (Huang et al. 2012; Li and Keh 2016) as well as air bubbles (Schnitzer et al. 2014) have been investigated. It is also a fact that in the practical applications, the shape of the particles is diverse. As a result, modeling of electrophoresis of spherical (Wiersema et al.

1966; Keh and Anderson 1985; Keh and Chiou 1996; Ennis and Anderson 1997; Shugai and Carnie 1999; Miloh and Boymelgreen 2014; Liu et al. 2016), cylindrical (Hsu and Ku 2005; Hsu et al. 2012a), rectangular (Li and Daghighi 2010; Movahed and Li 2012) or spheroidal (Yoon and Kim 1989) particles has been conducted.

Experimental studies of electrokinetic motion of single particles provide fundamental understanding of electrokinetic transport phenomena. For example, the channel wall effects on the electrokinetic motion of individual spherical microbeads in PDMS microchannels have been studied by Xuan et al. (2005, 2006). For transport of single nanoparticles in nanochannels, several numerical models (Liu et al. 2014; Hulings et al. 2015) were presented recently; however, systematic studies of electrokinetic motion of nanoparticles in nanopores or in straight nanochannels by experiments are very limited (Napoli et al. 2011; Han et al. 2012; Harms et al. 2015; Weerakoon-Ratnayake et al. 2016). One possible reason is that the nanochannels used in these studies are made of silicon, glass (Napoli et al. 2011; Harms et al. 2015) or thermal plastics (Weerakoon-Ratnayake et al. 2016), and high-cost, sophisticated equipment and complicated procedures are required for the device fabrication. In addition, the nanochannels used in these works are nanoslits that have only one dimension in the nanometer scale, while other dimensions of these nanoslits are larger than 5 µm (Napoli et al. 2011; Weerakoon-Ratnayake et al. 2016). Obviously, in these nanoslits, the nanoscale channel wall can influence the nanoparticle motion in one dimension. Furthermore, because of the micron size in other dimensions, such a nano-slit allows transport of multiple nanoparticles through the same cross section of the channel simultaneously, and the interactions between the nanoparticles may affect the electrophoretic mobility (Keh and Yang 1991; Keh and Chen 1993; Loewenberg and Davis 1995; Shugai et al. 1997; Ding and Keh 2001). Also, the ionic concentration of the buffer solutions is limited in a small range in these works, which is not sufficient to study the ionic concentration effects on the electrokinetic motion of nanoparticles. Electrophoresis of spherical nanoparticles in nanochannels with particle-to-nanochannel size ratio larger than 0.67 (Weerakoon-Ratnayake et al. 2016) is still a mystery.

This work investigates electrokinetic motion of single polystyrene nanoparticles in single PDMS nanochannels systematically. A novel method to fabricate PDMS-glass micro/nanochannel chips with single nanochannels smaller than 70 nm deep is presented. All the nanochannels used in this study are in nanoscale in both the width and the depth dimensions. Electrokinetic motion of single fluorescent nanoparticles in LiBr aqueous solutions from 10^{-5} to 10^{-2} M through single nanochannels is measured by a fluorescent particle tracking system. Concentration effects,

particle-to-channel size ratio effects, and electric field effects on the electrokinetic motion of single nanoparticles are investigated quantitatively. An extreme case of large size ratio (as large as 0.9) is also examined.

2 Experimental setup

2.1 Fabricating of micro/nanochannel chips

Reliable and reproducible micro-nanofluidic chips are essential to the experimental studies of electrokinetic motion of nanoparticles in nanochannels. The procedures for fabricating micro/nanochannel chips are as the following. Firstly, a nanocrack with desirable location and size is generated on a polystyrene surface by solvent-induced method (Peng and Li 2015, 2016a). An artificial defect marked on the polystyrene surface is used to control the location of the nanocrack, and the location of the defect is controlled by the manipulation stage of a microhardness testing system (Peng and Li 2016a), and the size of the nanocrack is adjusted by controlling the working parameters of the solvent-induced method, i.e., the volume of the reagent, the heating time, the heating temperature and so on (Peng and Li 2015). Then, the negative nanocrack is replicated onto a piece of polymer slab (Smooth cast) surface by applying the nanoimprint method, and the

optimal working parameters for this process can be found in the reference (Peng and Li 2016a). In the third step, a piece of PDMS slab with microchannel system composed of one pair of U-shaped negative microchannels is attached to another layer of flat PDMS slab. The PDMS slab with the microchannel system is replicated from a microchannel mold which is fabricated by the standard photolithography technique. The hollow microchannels are filled with liquid-form pre-curing smooth cast first. Then, the flat PDMS slab is peeled off after 30 min, leaving the rubber-like smooth cast inside the microchannels. After that, the PDMS slab with microchannels is attached to the plasma-treated smooth cast nanochannel mold that is positioned to bridge the two U-shaped microchannels. The smooth cast microchannel will be bonded onto the nanochannel mold surface due to the plasma treatment. Finally, a smooth cast micro/nanochannel mold is obtained by peeling off the PDMS microchannel. The smooth cast micro-nanofluidic channel mold is used to replicate the network of two U-shaped microchannels bridged by a nanochannel in a PDMS chip by applying the bilayer strategy, with one thin layer of x-PDMS supported by a thick layer of regular PDMS (Peng and Li 2016a). Finally, a nanofluidic chip is obtained by bonding the PDMS micro/nanochannel chip onto a piece of glass slide after plasma treatment. Figure 1a shows an example of the micro/nanochannel chips, and Fig. 1b is a zoomed-in view of the nanochannel section. Figure 1c, d


Fig. 1 **a** An example of the PDMS-glass micro/nanochannel chips, **b** a zoomed-in view of the micro/nanochannel conjunctions of the micro/nanochannel chip, **c** a 3D image of the nanochannel and **d** three cross sections *A*, *B* and *C* of this nanochannel, separated by 3 μm measured by the AFM. The nanochannel is about 610 nm wide and 180 nm deep
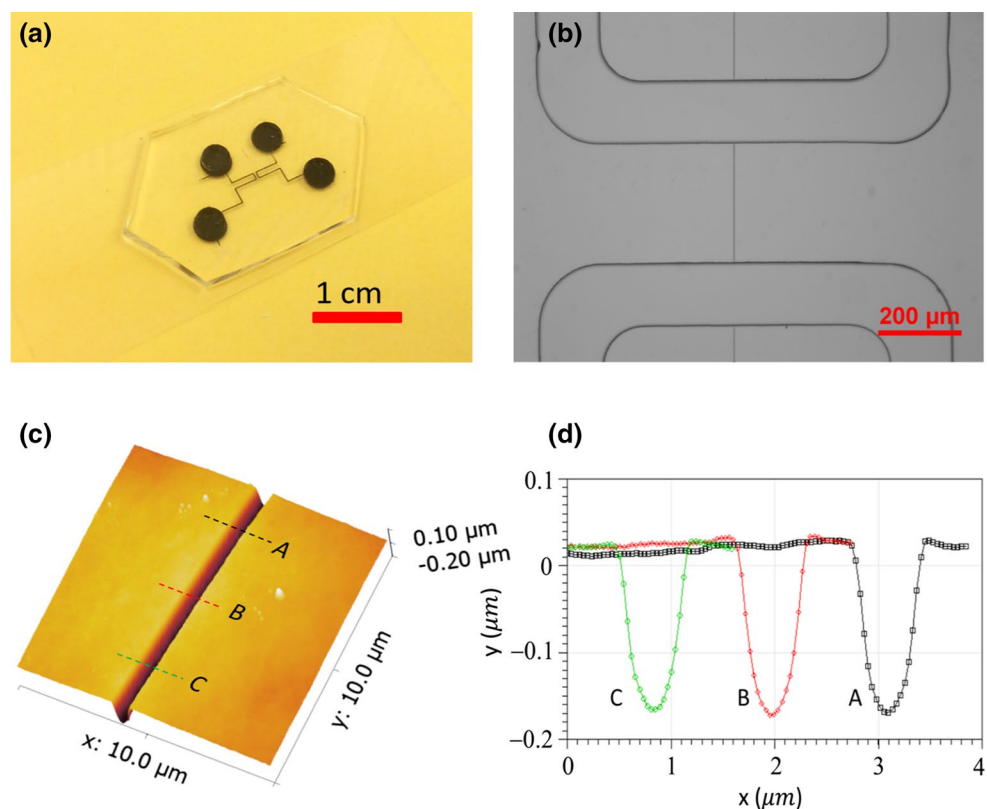
is a 3D image of the nanochannel and three cross sections of this nanochannel measured by an AFM (Multimode™ SPM, Digital Instruments), respectively.

2.2 Fluorescent nanoparticle tracking system

One direct way to determine the velocity of a fluorescent nanoparticle is to track the motion of the fluorescent nanoparticle by using a fluorescent microscope. Figure 2a shows a schematic diagram of the nanoparticle tracking system used in this study. This system is composed of a fluorescent microscope (Nikon Ti-E), a PDMS-glass micro-nanofluidic chip, a DC power source and a computer with image processing software (NIS-Elements BR). The fluorescent microscope is equipped with a $100\times$ oil immersion objective lens (Apo λ, NA = 1.45), a blue laser source (λ = 488 nm) and a CCD camera (Q-imaging, Retiga 2000R). During the experiments, the micro/nanochannel chip is located on the working stage of the microscope with the nanochannel section on the focal point of the oil
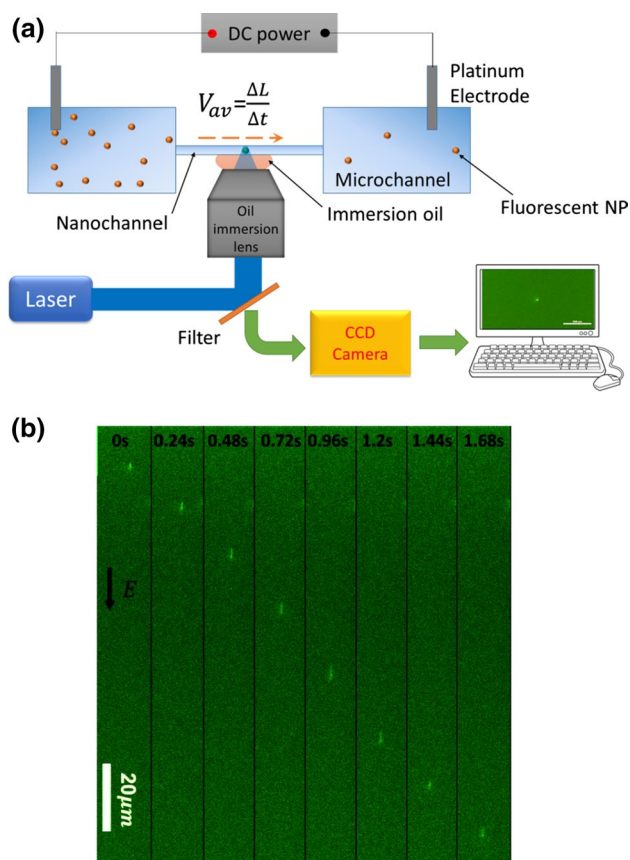
lens. Nanoparticle samples are loaded into the microchannels and the nanochannel through the channel wells. A DC power source (Keithley, 6517A) is employed to apply electrical field along the single nanochannel through two Platinum electrodes inserted in the wells at the end of the microchannels. In this way, nanoparticles are loaded into the nanochannel by electroosmotic flow. As the nanoparticles move in the nanochannels under the electric fields, the CCD camera will record the motion of the nanoparticles and the software will calculate the apparent velocity of the particles. Figure 2b shows an example of the trajectory of a 140-nm particle in a 340-nm-deep nanochannel under an electric field of 2 kV/m. The nanoparticle is in 10^{-4} M LiBr solution, and the average apparent velocity of this nanoparticle is 68.5 µm/s. A video of the particle motion can be found in the Electronic Supplementary Material.

In this work, in order to study the electrokinetic motion of single nanoparticles in single nanochannels, only one single nanoparticle was introduced into the nanochannel each time. However, for most cases, both the PDMS nanochannel wall and the nanoparticles are negatively charged. As a result, the nanoparticles can hardly flow into the nanochannel freely even an external electric field (for example, 2 kV/m in the experiments) was applied along the nanochannel due to electrostatic repulsion between the channel wall and the nanoparticles. However, nanoparticle will accumulate at the entrance of the nanochannel due to the electrostatic attraction force. To "push" the nanoparticles into the nanochannel, a very strong electric field pulse (duration of less than 0.5 s) was applied to the nanochannel; consequently, one or more nanoparticles were introduced into the nanochannel in a very short time due to the strong electrostatic force along the axis of the nanochannel. In the case of more than one nanoparticles were loaded into the nanochannel, a weak electric field was applied on the nanochannel to release some of the particles, finally leaving only one inside the channel. It should be noted that, because the nanochannels are in nanoscale in both the depth and the width directions, the nanoparticles inside the nanochannel will line up automatically due to the above-mentioned electrostatic repulsion force between the channel wall and the nanoparticles. As a result, the releasing process can be controlled precisely. As only one nanoparticle was introduced into the channel, we switched the direction of the electric field of specific value back and forth to drive or manipulate the single nanoparticle and to measure the electrokinetic velocity, generally, for 10 time or more. After that, this particle was released, and another one was loaded, and so on and so forth.

2.3 Chemical reagents and experimental setup

The particle-solution samples were prepared by diluting green carboxylated polystyrene fluorescent nanoparticles

Fig. 2 a Schematic of the fluorescent particle tracking system, and **b** an example of electrokinetic motion of a 140-nm particle in a 340-nm-deep nanochannel under 20 V/cm electric field. The video was captured by a CCD camera (Q-imaging, Retiga 2000R) with an exposure time setting of 80 ms

(Bangs Laboratories Inc.) into LiBr solutions. The particle concentration used in the experiments is diluted to about 10^9/mL. Three sizes of nanoparticles, 60, 83 and 140 nm, are used in this study. The ionic concentrations of LiBr solutions used in this work include 10^{-5}, 10^{-4}, 10^{-3} and 10^{-2} M. The buffer solutions were obtained by dissolving LiBr (Fisher Scientific) into pure water (Mini Q, Direct-Q3, 18.2 MΩ cm). The length of the nanochannels is 300 μm. DC electric fields from 1 to 10 kV/m were applied over the 300-μm-long nanochannels. To study the particle-to-channel size ratio effects on the electrokinetic motion of nanoparticles, six nanochannels and two straight microchannels were fabricated. Table 1 gives the details of the channels. All the channels are measured by the microscope or the AFM for at least five times. Chip conditioning is conducted by loading LiBr solutions into the fresh channels for 15 min before nanoparticle samples are loaded. It should be noted that the buffer solution used for the chip conditioning is the same as that of the nanoparticle sample solutions. For each working condition, i.e., one channel size, one particle size, one ionic concentration and one electric field, the experiments were repeated for at least three times on three independent fresh chips; and for each chip, the motion of the nanoparticles was tracked for at least ten times. The motion of the nanoparticles was captured by the CCD camera with an exposure time setting of 80–150 ms. For large nanoparticles, for example, 140-nm nanoparticles, the fluorescent light intensity is high and the exposure time setting was relatively short, 80 ms; however, for smaller nanoparticles, for example, 60-nm nanoparticles, the exposure time setting was longer (150 ms) to make sure the accuracy of the measurement. All the experiments were conducted at room temperature of about 25 °C. For all the cases, only the apparent velocity was measured. The apparent velocity is the combined result of the electrophoresis velocity of the particle and the velocity of the electroosmotic flow inside the channel and is more useful for the practical applications.

Table 1 Sizes of the PDMS-glass microchannels and the PDMS-glass nanochannels

Channel no.	Width (w)	Depth (b)
1	50 μm	25 μm
2	10 μm	5 μm
3	501 ± 24 nm	340 ± 17 nm
4	460 ± 15 nm	157 ± 13.5 nm
5	436 ± 18 nm	102 ± 5.6 nm
6	596 ± 11 nm	91 ± 5 nm
7	450 ± 25 nm	83 ± 6.5 nm
8	507 ± 11 nm	67 ± 3 nm

3 Results and discussion

3.1 Ionic concentration effects

Nanoparticles of 60 and 140 nm in diameter in 10^{-2}, 10^{-3}, 10^{-4} and 10^{-5} M LiBr solutions were tested in two nanochannels with cross sections of 340×501 nm and 157×460 nm, respectively, as well as in a microchannel with a cross section of 25×50 μm, with an applied electric field of 2 kV/m. The apparent velocity of the 60- and 140-nm nanoparticles is showing in Fig. 3, in which a is the diameter of the nanoparticles and b is the depth of the channels. From Fig. 3 one can see that in the microchannel, the apparent velocity of 140-nm nanoparticles increases with the decreasing ionic concentration from 45 to 110 μm/s, which is consistent with the dependence of the electroosmotic flow on the ionic concentration (Peng and Li 2016b). The increase in the electroosmotic flow is due to the increase in zeta potential of the microchannel wall surfaces. However, the zeta potential of the nanoparticles also increases with the decreasing ionic concentration. From the results one can conclude that the influence of the increase in particle zeta poetical is minor and the apparent velocity of the nanoparticles is dominated by the electroosmotic flow in the channel.
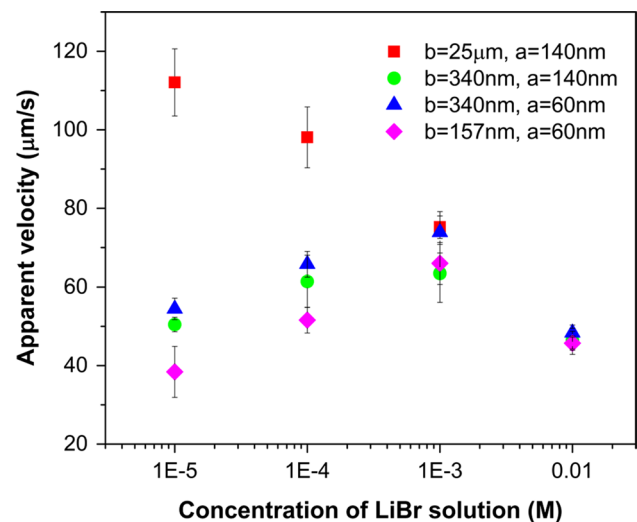
Fig. 3 Concentration effects on the electrokinetic velocity of single nanoparticles in single nanochannels. Apparent velocity of 60-nm particles and 140-nm nanoparticles in single nanochannels of 340×501 nm cross section and, 157×460 nm cross section, and in a microchannel of 25×50 μm was measured by the particle tracking system. For all the cases, the electric field applied over the nanochannels and the microchannel is 2 kV/m and the ionic concentrations of the LiBr solution are 10^{-2}, 10^{-3}, 10^{-4} and 10^{-5} M, and for each data point, the experiments were repeated for at least 30 times. Here, a is the diameter of the nanoparticles, and b is the depth of channels
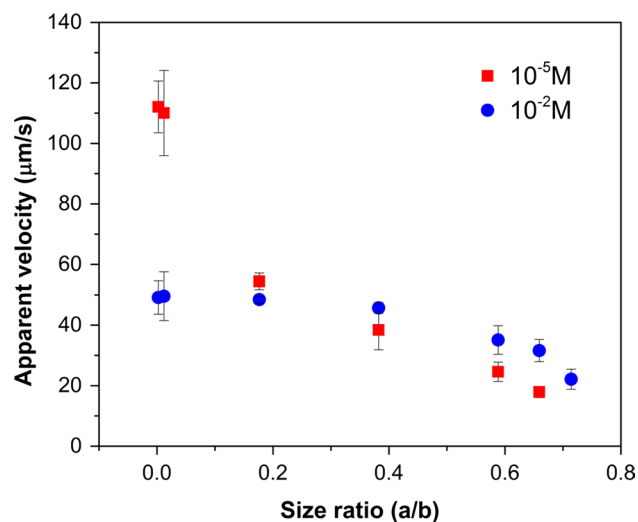
In the two nanochannels, the apparent velocity of both 60- and 140-nm nanoparticles increases as the ionic concentration decreases from 10^{-2} to 10^{-3} M. However, as the ionic concentration decreases further, the velocity of both the 60- and 140-nm nanoparticles experiences a decreasing trend, which is opposite to that in the microchannel. Obviously, for the cases of 10^{-2} and 10^{-3} M solutions in nanochannels, the thickness of the EDL is very thin, about 10 and 40 nm, respectively; as a result, there is no overlap of EDLs in these two nanochannels, the electroosmotic flow in these two nanochannels is the same as that in the microchannel, increasing with the decrease in ionic concentration, similar to that in the microchannel as mentioned above. By contrast, as the ionic concentration decreases further, to 10^{-4} and 10^{-5} M, the thickness of the EDL adjacent to the channel walls increases dramatically, to about 120 and 400 nm respectively; as a consequence, EDLs are overlapped in the two nanochannels, resulting in a decreasing electroosmotic flow inside the nanochannels. The effects of overlap of EDLs on the electroosmotic flow in nanochannels can be found in the literature (Peng and Li 2016b). In addition, as the ionic concentration decreases, the increase in zeta potential of the polystyrene nanoparticles will also give rise to larger electrophoretic mobility values of the nanoparticles, but in the opposite direction of the electroosmotic flow. As a result, the apparent velocity decreases further, to about 38 and 55 μm/s for the cases of 60-nm particles in the 157-nm-deep and 340-nm-deep nanochannels with 10^{-5} M ionic concentration environment.

Interactions between the EDLs of the nanochannels and the nanoparticles affect the apparent velocity of the nanoparticles. As the ionic concentration decreases, the thickness of EDL near both the nanochannel walls and the nanoparticle surface increases and EDLs may overlap in the gaps between the nanochannel walls and the nanoparticles easily, especially for the cases of large particle-to-channel size ratio systems. For example, in the case of 157-nm nanochannel loaded with 60-nm nanoparticles in 10^{-3} M LiBr solution, no overlap of EDL of the opposite nanochannel walls, because the thickness of the EDL is about 40 nm which is much smaller than the half depth of the nanochannel, about 80 nm. However, if a 60-nm nanoparticle was loaded in this nanochannel, the gap between the nanoparticle surface and the channel wall should be around 50 nm, assuming that the nanoparticle is located in the middle of the nanochannel due to EDL repulsion (Liu et al. 2014). Consequently, the thickness of the EDL, 40 nm, is larger than the half length of the gap, 25 nm, which means EDLs get overlapped between the nanoparticle and the nanochannel walls. As seen in Fig. 3, the apparent velocity of the 60-nm nanoparticle is smaller than that in the microchannel. For the cases of particle motion in an overlap EDL, it is hard to find an analytical solution for the nanoparticle transport behavior due to the

sophisticated interactions between the particle and the channel wall. However, compared with the cases without overlap of EDL mentioned above, the zeta potential changes are the same, and only the overlap EDL matters. Consequently, we can predict that the electrokinetic motion of nanoparticles in nanochannels filling with diluted ionic solutions is dominated by the overlap EDL and also the overlapping of EDLs between the nanoparticle and the nanochannel walls under the condition of low ionic concentration contributes to a smaller apparent velocity.

3.2 Effects of particle-to-channel size ratio

Figure 4 depicts the channel size effects on the electrokinetic motion of 60-nm nanoparticles in nanochannels of 340, 157, 102, 91 and 84 nm in depth as well as in microchannels of 25 and 5 μm in depth with 10^{-2} and 10^{-5} M LiBr solution environment. The applied electric field is 2 kV/m for all the cases. In Fig. 4, the size ratio a/b is plotted as the x-axis, where a is the diameter of the nanoparticle and b is the depth of the channels. It is obvious that the apparent velocity of the nanoparticles decreases with the size ratio for both concentration values. For instance, for the 10^{-2} M cases, the apparent velocity of 60-nm nanoparticles in the microchannels ($a/b \approx 0$) and large nanochannels (340-nm-deep nanochannel, $a/b = 0.18$) is about 50 μm/s; however, as the channel size decreases to 84 nm deep ($a/b = 0.71$), the apparent velocity decreases gradually to about 22 μm/s.


Fig. 4 Particle-to-channel size ratio effects on the apparent velocity of 60-nm nanoparticle in nanochannels of 340, 157, 102, 91 and 84 nm in depth as well as in microchannels of 25 and 5 μm in depth with 10^{-2} and 10^{-5} M LiBr solution, where a is the diameter of the nanoparticles and b is the depth of the channels. The applied electric field is 2 kV/m m for all the cases, and for each case, the experiments were repeated for at least 30 times

Similarly, for the cases of 10^{-5} M ionic concentration, the velocity of 60-nm nanoparticles in the microchannels is about 110 µm/s; however, when the channel size decreases down to nanometer scale ($a/b > 0.18$ in Fig. 4), the apparent velocity of the nanoparticles decreases dramatically due to interactions between EDLs, because the thickness of the EDL for the 10^{-5} M case is very large, is about 400 nm, and EDLs are overlapped between nanochannel walls and also between the nanochannel walls and the nanoparticles. When EDLs get overlapped, the electroosmotic flow in the nanochannel will decrease, and the interactions between the nanoparticles and the channel walls become stronger; consequently, the apparent velocity decreases rapidly with the channel size. For example, the velocity of the 60-nm nanoparticles is about 55 µm/s in the 340-nm-deep nanochannel ($a/b = 0.18$), and this value decreases to about 20 µm/s as the channel size decreases to 91 nm ($a/b = 0.66$), in which EDLs get overlapped strongly. It can be concluded that, as channel size becomes smaller and the size ratio becomes larger, interactions between the EDLs will dominate the electrokinetic motion of the nanoparticles, resulting in a decrement of the apparent velocity.

It should be noted, under the condition of strong EDL interactions, for example, for the case of 60-nm nanoparticles in an 84-nm-deep nanochannel ($a/b = 0.71$) filled with 10^{-5} M LiBr solution, the nanoparticles can hardly move under low electric fields. Aggregation occurs in the nanochannel due to the strong particle–nanochannel electrostatic interactions. An example of 60-nm nanoparticles trapped in an 84-nm-deep nanochannel is shown in Fig. S1a of the Electronic Supplementary Material. The nanoparticles can only be removed with very high electric field (10^6 V/m or higher). Trapping of DNAs inside nanopores under the condition of low electric field has also been reported (Ai et al. 2010). Attempt of transporting 60-nm nanoparticles in a 67-nm-deep nanochannel ($a/b \approx 0.9$) indicates that it is extremely hard to load 60-nm nanoparticles into such a small nanochannel by electroosmotic flow due to strong DEP (dielectrophoresis) force at the channel entrance (Dongqing Li 2008) or the electrostatic repulsion force between the nanoparticles and the channel wall surfaces. Generally, 60-nm nanoparticles are stuck at the entrance of the 67-nm nanochannel, as shown in Fig. S1b.

3.3 Electric field effects

Figure 5 depicts the electric field effects on the apparent velocity of 60-nm nanoparticles in a 157-nm-deep nanochannel filled with 10^{-2} M buffer solution, 140-nm particles in a 25-µm-deep microchannel filled with 10^{-2} M buffer solution and 140-nm particles in a 340-nm-deep nanochannel loaded with 10^{-3} M LiBr solution, respectively. The electric field ranges from 1 to 10 kV/m. It is
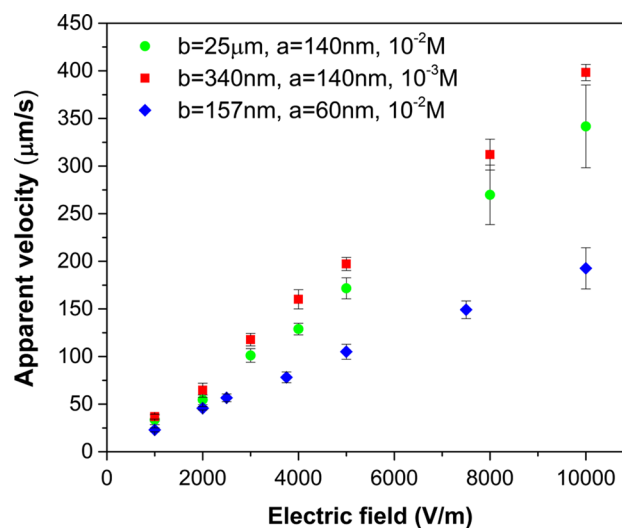
Fig. 5 Electric field effects on the apparent velocity of 60-nm nanoparticles in a 157-nm-deep nanochannel filled with 10^{-2} M LiBr solution, and 140-nm nanoparticles in a 25-µm-deep microchannel filled with 10^{-2} M LiBr solution and in a 340-nm-deep nanochannel loaded with 10^{-3} M LiBr solution. The applied electric field ranges from 1 to 10 kV/m, and for each case, the experiments were repeated for at least 30 times

obvious that the apparent velocity of the nanoparticles increases almost linearly with the applied electric field for all the cases. The slopes of these curves indicate the mobility values of these particles. From Fig. 5 one can see that in 10^{-2} M LiBr solution, the motion of 60-nm nanoparticles in the nanochannel of 157 nm deep is smaller than that of 140-nm particles in the 25-µm-deep microchannel due to the interactions of the overlapped EDLs as mentioned above. In addition, electrokinetic motion of 140-nm nanoparticles in the 25-µm-deep microchannel filled with 10^{-2} M LiBr solution is smaller than that in the 340-nm-deep nanochannel filled with 10^{-3} M LiBr solution. This is because the electroosmotic flow in the channel is much weaker in the high ionic concentration (10^{-2} M) solution. In Fig. 5, under the condition of higher electric fields, the error bars of the measured velocity are larger compared with that of the low electric field cases due to the limitation of the fluorescent tracking system. Under the condition of a high electric field, the velocity of the fluorescent particles is high and a sufficient exposure time is needed to clearly observe the nanoparticles. However, a longer exposure time makes the trajectories of the nanoparticles blurring and results in larger errors during the velocity calculation. "Stick/slip" motion of the nanoparticles under the conditions of low electric field and large size ratio has also been observed during the experiments, as shown in Fig. S1a. The "stick/slip" motion was previously observed in the experimental studies of translocation of DNAs through nanochannels probably due to strong electrostatic interactions

between the negatively charged DNAs and the positively charged channel wall (Uba et al. 2015). However, in this case, both the nanochannel wall and the nanoparticles are negatively charged, the "stick/slip" behavior may due to strong inhomogeneous electric field inside the channel caused by the surface roughness of the nanochannel wall.

4 Conclusions

This paper presents a systematical experimental study of electrokinetic motion of single nanoparticles in single nanochannels. PDMS-glass micro/nanochannel chips with single nanochannels are developed. The effects of ionic concentration, particle-to-channel size ratio (a/b) and electric field on the apparent velocity of electrophoretic motion fluorescent nanoparticles in six nanochannels and two microchannels by particle tracking method are investigated. The results show that the electrokinetic velocity of nanoparticles in small single nanochannels increases with the ionic concentration in diluted solutions ($<10^{-3}$ M) and decreases with the ionic concentration in concentrated solutions ($>10^{-3}$ M). The apparent velocity of single nanoparticles in single nanochannels decreases with increasing particle-to-channel size ratio (a/b) due to the interactions of the overlapped EDLs inside the nanochannels. Under the condition of a proper electric field range, the apparent velocity increases with the applied electric field linearly. "Stick–slip" motion and stuck of nanoparticles in single nanochannels under the conditions of large size ratio and low electric field have also been observed. The experimental study presented in this article provides improved understanding of electrokinetic motion of nanoparticles in nanospaces and is potentially valuable for the future applications nanofluidics.

References

Ai Y, Liu J, Zhang B, Qian S (2010) Field effect regulation of DNA translocation through a nanopore. Anal Chem 82:8217–8225

Chen SB, Keh HJ (1988) Electrophoresis in a dilute dispersion of colloidal spheres. AIChE J 34:1075–1085. doi:10.1002/aic.690340704

Chen WJ, Keh HJ (2013) Electrophoresis of a charged soft particle in a charged cavity with arbitrary double-layer thickness. J Phys Chem B 117:9757–9767. doi:10.1021/jp405357e

Davenport M, Healy K, Pevarnik M et al (2012) The role of pore geometry in single nanoparticle detection. ACS Nano 6:8366–8380. doi:10.1021/nn303126n

Delgado AV, González-Caballero F, Hunter RJ et al (2007) Measurement and interpretation of electrokinetic phenomena. J Colloids Interface Sci 309:194–224. doi:10.1016/j.jcis.2006.12.075

Ding JM, Keh HJ (2001) The electrophoretic mobility and electric conductivity of a concentrated suspension of colloidal spheres with arbitrary double-layer thickness. J Colloids Interface Sci 236:180–193. doi:10.1006/jcis.2000.7383

Duan C, Wang W, Xie Q (2013) Fabrication of nanofluidic devices. Biomicrofluidics 7:26501. doi:10.1063/1.4794973

Dukhin SS (1993) Non-equilibrium electric surface phenomena. Adv Colloids Interface Sci 44:1–134. doi:10.1016/0001-8686(93)80021-3

Ennis J, Anderson J (1997) Boundary effects on electrophoretic motion of spherical particles for thick double layers and low zeta potential. J Colloids Interface Sci 185:497–514. doi:10.1006/jcis.1996.4596

Fu J, Schoch RB, Stevens AL et al (2007) A patterned anisotropic nanofluidic sieving structure for continuous-flow separation of DNA and proteins. Nat Nanotechnol 2:121–128

Han R, Wang G, Qi S et al (2012) Electrophoretic migration and axial diffusion of individual nanoparticles in cylindrical nanopores. J Phys Chem C 116:18460–18468. doi:10.1021/jp303855d

Harms ZD, Haywood DG, Kneller AR et al (2015) Single-particle electrophoresis in nanochannels. Anal Chem 87:699–705. doi:10.1021/ac503527d

Henry DC (1931) The cataphoresis of suspended particles. Part I. The equation of cataphoresis. In: Proceedings of the royal society of London A: mathematical, physical and engineering sciences. The royal society, pp 106–129

Hsu J-P, Chen Z-S (2007) Electrophoresis of a sphere along the axis of a cylindrical pore: effects of double-layer polarization and electroosmotic flow. Langmuir 23:6198–6204

Hsu JP, Ku MH (2005) Boundary effect on electrophoresis: finite cylinder in a cylindrical pore. J Colloids Interface Sci 283:592–600. doi:10.1016/j.jcis.2004.09.004

Hsu JP, Ku MH, Kao CY (2004) Electrophoresis of a spherical particle along the axis of a cylindrical pore: effect of electroosmotic flow. J Colloids Interface Sci 276:248–254. doi:10.1016/j.jcis.2004.03.025

Hsu JP, Lo HM, Yeh LH, Tseng S (2012a) Importance of boundary on the electrophoresis of a soft cylindrical particle. J Phys Chem B 116:12626–12632. doi:10.1021/jp305473s

Hsu JP, Yee CP, Yeh LH (2012b) Importance of electroosmotic flow and multiple ionic species on the electrophoresis of a rigid sphere in a charge-regulated zwitterionic cylindrical pore. Langmuir 28:10942–10947. doi:10.1021/la3018634

Huang C-H, Hsu H-P, Lee E (2012) Electrophoretic motion of a charged porous sphere within micro- and nanochannels. Phys Chem Chem Phys 14:657–667. doi:10.1039/C1CP21938C

Hulings ZK, Melnikov DV, Gracheva ME (2015) Charged nanoparticle in a nanochannel: competition between electrostatic and dielectrophoretic forces. Phys Rev E Stat Nonlinear Soft Matter Phys 91:1–7. doi:10.1103/PhysRevE.91.062713

Jeffet J, Kobo A, Su T et al (2016) Super-resolution genome mapping in silicon nanochannels. ACS Nano. doi:10.1021/acsnano.6b05398

Keh H, Anderson J (1985) Boundary effects on electrophoretic motion of colloidal spheres. J Fluid Mech 153:417–439

Keh H, Chen S (1988) Electrophoresis of a colloidal sphere parallel to a dielectric plane. J Fluid Mech 194:377–390

Keh HJ, Chen JB (1993) Particle interactions in electrophoresis. 5. Motion of multiple spheres with thin but finite electrical double-layers. J Colloids Interface Sci 158:199–222. doi:10.1006/jcis.1993.1248

Keh HJ, Chiou JY (1996) Electrophoresis of a colloidal sphere in a circular cylindrical pore. AIChE J 42:1397–1406. doi:10.1002/aic.690420520

Keh HJ, Hsieh TH (2008) Electrophoresis of a colloidal sphere in a spherical cavity with arbitrary zeta potential distributions

and arbitrary double-layer thickness. Langmuir 24:390–398. doi:10.1021/la702399u

Keh HJ, Yang FR (1991) Particle interactions in electrophoresis. 4. Motion of arbitrary 3-dimensional clusters of spheres. J Colloids Interface Sci 145:362–389

Lee TC, Keh HJ (2014) Electrophoresis of a spherical particle in a spherical cavity. Microfluid Nanofluidics 16:1107–1115. doi:10.1007/s10404-013-1276-8

Li D (2004) Electrokinetics in microfluidics. Academic Press, Cambridge

Li D (2008) Encyclopedia of microfluidics and nanofluidics. Springer, New York

Li D, Daghighi Y (2010) Eccentric electrophoretic motion of a rectangular particle in a rectangular microchannel. J Colloids Interface Sci 342:638–642. doi:10.1016/j.jcis.2009.10.047

Li WC, Keh HJ (2016) Electrophoretic mobility of charged porous shells or microcapsules and electric conductivity of their dilute suspensions. Colloids Surfaces A Physicochem Eng Asp 497:154–166. doi:10.1016/j.colsurfa.2016.02.028

Liu YW, Pennathur S, Meinhart CD (2014) Electrophoretic mobility of a spherical nanoparticle in a nanochannel. Phys Fluids. doi:10.1063/1.4901330

Liu YW, Pennathur S, Meinhart CD (2016) Electrophoretic mobility of spherical particles in bounded domain. J Colloids Interface Sci 461:32–38. doi:10.1016/j.jcis.2015.08.039

Loewenberg M, Davis RH (1995) Near-contact electrophoretic particle motion. J Fluid Mech 288:103. doi:10.1017/S002211209500108X

Masliyah JH, Bhattacharjee S (2006) Electrokinetic and colloid transport phenomena. Wiley, Hoboken

Menard LD, Ramsey JM (2013) Electrokinetically-driven transport of DNA through focused ion beam milled nano fluidic channels. Anal Chem 85:1146–1153

Mijatovic D, Eijkel JCT, van den Berg A (2005) Technologies for nanofluidic systems: top–down vs. bottom–up—a review. Lab Chip 5:492–500. doi:10.1039/b416951d

Miloh T, Boymelgreen A (2014) Travelling wave dipolophoresis of ideally polarizable nano-particles with overlapping electric double layers in cylindrical pores. Phys Fluids. doi:10.1063/1.4884956

Movahed S, Li D (2012) Electrokinetic motion of a rectangular nanoparticle in a nanochannel. J Nanoparticle Res 14:1–15. doi:10.1007/s11051-012-1032-0

Napoli M, Eijkel JCT, Pennathur S (2010) Nanofluidic technology for biomolecule applications: a critical review. Lab Chip 10:957–985. doi:10.1039/b917759k

Napoli M, Atzberger P, Pennathur S (2011) Experimental study of the separation behavior of nanoparticles in micro- and nano-channels. Microfluid Nanofluidics 10:69–80. doi:10.1007/s10404-010-0647-7

Nedelcu S, Sommer JU (2014) Charge inversion effects in electrophoresis of polyelectrolytes in the presence of multivalent counterions and transversal electric fields. Polymers (Basel) 6:2942–2960. doi:10.3390/polym6122942

O'Brien RW, Hunter RJ (1981) The electrophoretic mobility of large colloidal particles. Can J Chem 59:1878–1887. doi:10.1139/v81-280

O'Brien RW, White LR (1978) Electrophoretic mobility of a spherical colloidal particle. J Chem Soc Faraday Trans 2 Mol Chem Phys 74:1607–1626

Ohshima H (1994) A simple expression for henry's function for the retardation effect in electrophoresis of spherical colloidal particles. J Colloids Interface Sci 168:269–271

Ohshima H (1995a) Electrophoresis of soft particles. Adv Colloids Interface Sci 62:189. doi:10.1016/0001-8686(95)00279-Y

Ohshima H (1995b) Electrophoretic mobility of soft particles. Colloids Surf A Physicochem Eng Asp 103:249–255. doi:10.1016/0927-7757(95)03293-M

Ohshima H (1996) Henry's function for electrophoresis of a cylindrical colloidal particle. J Colloids Interface Sci 180:299–301. doi:10.1006/jcis.1996.0305

Ohshima H, Healy TW, White LR (1983) Approximate analytic expressions for the electrophoretic mobility of spherical colloidal particles and the conductivity of their dilute suspensions. J Chem Soc Faraday Trans 2 Mol Chem Phys 79:1613–1628

Peng R, Li D (2015) Fabrication of nanochannels on polystyrene surface. Biomicrofluidics 9:24117. doi:10.1063/1.4918643

Peng R, Li D (2016a) Fabrication of polydimethylsiloxane (PDMS) nanofluidic chips with controllable channel size and spacing. Lab Chip 16:3767–3776. doi:10.1039/C6LC00867D

Peng R, Li D (2016b) Electroosmotic flow in single PDMS nanochannels. Nanoscale. doi:10.1039/C6NR02937J

Plesa C, Verschueren D, Pud S et al (2016) Direct observation of DNA knots using a solid-state nanopore. Nat Nanotechnol. doi:10.1038/nnano.2016.153

Qian S, Joo SW, Hou W, Zhao X (2008) electrophoretic motion of a spherical particle with a symmetric nonuniform surface charge distribution in a nanotube. Langmuir 24(10):5332–5340

Sackmann EK, Fulton AL, Beebe DJ (2014) The present and future role of microfluidics in biomedical research. Nature 507:181–189. doi:10.1038/nature13118

Schnitzer O, Frankel I, Yariv E (2014) Electrophoresis of bubbles. J Fluid Mech 753:49–79. doi:10.1017/jfm.2014.350

Semenov I, Raafatnia S, Sega M et al (2013) Electrophoretic mobility and charge inversion of a colloidal particle studied by single-colloid electrophoresis and molecular dynamics simulations. Phys Rev E Stat Nonlinear Soft Matter Phys 87:1–7. doi:10.1103/PhysRevE.87.022302

Shugai A, Carnie S (1999) Electrophoretic motion of a spherical particle with a thick double layer in bounded flows. J Colloids Interface Sci 213:298–315. doi:10.1006/jcis.1999.6143

Shugai AA, Carnie SL, Chan DYC, Anderson JL (1997) Electrophoretic motion of two spherical particles with thick double layers. J Colloids Interface Sci 371:357–371

Swan JW, Furst EM (2012) A simpler expression for Henry's function describing the electrophoretic mobility of spherical colloids. J Colloids Interface Sci 388:92–94. doi:10.1016/j.jcis.2012.08.026

Tseng S, Lin C, Hsu J, Yeh L (2013) Electrophoresis of deformable polyelectrolytes in a nanofluidic channel. Langmuir 29:2446–2454

Uba FI, Pullagurla SR, Sirasunthorn N et al (2015) Surface charge, electroosmotic flow and DNA extension in chemically modified thermoplastic nanoslits and nanochannels. Analyst 140:113–126. doi:10.1039/c4an01439a

Unlu M, Morgan ME, Minden JS (1997) Difference gel electrophoresis: a single gel method for detecting changes in protein extracts. Electrophoresis 18:2071–2077. doi:10.1002/elps.1150181133

Wang LJ, Keh HJ (2009) Electrophoresis of a cylindrical particle with a nonuniform zeta potential distribution parallel to a charged plane wall. J Phys Chem C 113:12790–12798. doi:10.1021/jp903077e

Wang YC, Stevens AL, Han J (2005) Million-fold preconcentration of proteins and peptides by nanofluidic filter. Anal Chem 77:4293–4299. doi:10.1021/ac050321z

Wang N, Yee CP, Chen YY et al (2013) Electrophoresis of a pH-regulated zwitterionic nanoparticle in a pH-regulated zwitterionic capillary. Langmuir 29:7162–7169. doi:10.1021/la400946s

Weerakoon-Ratnayake KM, Uba FI, Oliver-Calixte NJ, Soper SA (2016) Electrophoretic separation of single particles using nanoscale thermoplastic columns. Anal Chem 88:3569–3577. doi:10.1021/acs.analchem.5b04065

Wiersema P, Loeb A, Overbeek JT (1966) Calculation of the electrophoretic mobility of a spherical colloid particle. J Colloids Interface Sci 22:78–99. doi:10.1016/0021-9797(66)90069-5

Xia D, Yan J, Hou S (2012) Fabrication of nanofluidic biochips with nanochannels for applications in DNA analysis. Small 8:2787–2801. doi:10.1002/smll.201200240

Xuan X, Ye C, Li D (2005) Near-wall electrophoretic motion of spherical particles in cylindrical capillaries. J Colloids Interface Sci 289:286–290. doi:10.1016/j.jcis.2005.03.045

Xuan X, Raghibizadeh S, Li D (2006) Wall effects on electrophoretic motion of spherical polystyrene particles in a rectangular poly(dimethylsiloxane) microchannel. J Colloids Interface Sci 296:743–748. doi:10.1016/j.jcis.2005.09.039

Yasui T, Rahong S, Motoyama K et al (2013) DNA manipulation and separation in sublithographic-scale nanowire array. ACS Nano 7:3029–3035

Yoon BJ, Kim S (1989) Electrophoresis of spheroidal particles. J Colloids Interface Sci 128:275–288. doi:10.1016/0021-9797(89)90405-0

Zhang X, Hsu WL, Hsu JP, Tseng S (2009) Diffusiophoresis of a soft spherical particle in a spherical cavity. J Phys Chem B 113:8646–8656. doi:10.1021/jp9014417

Zhou K, Perry JM, Jacobson SC (2011) Transport and sensing in nanofluidic devices. Annu Rev Anal Chem 4:321–341. doi:10.1146/annurev-anchem-061010-113938